

**An Ensemble of Models of the Acute Inflammatory Response to
Bacterial Lipopolysaccharide in Rats: Results from Parameter Space
Reduction**

Silvia Daun^{a,b,c}, Jonathan Rubin^{b,c}, Yoram Vodovotz^{b,d}, Anirban Roy^e, Robert
Parker^e, Gilles Clermont^{a,b,*}

^a Department of Critical Care Medicine, 3550 Terrace St, University of
Pittsburgh, Pittsburgh, Pennsylvania, 15261

^b Center for Inflammation and Regenerative Modeling, 100 Technology Drive,
University of Pittsburgh, Pittsburgh, Pennsylvania, 15219

^c Department of Mathematics, 301 Thackeray Hall, University of Pittsburgh,
Pittsburgh, Pennsylvania, 15260

^d Department of Surgery, 200 Lothrop St, University of Pittsburgh, Pittsburgh,
Pennsylvania, 15213

^e Department of Chemical and Petroleum Engineering, 1241 Benedum Hall, University
of Pittsburgh, Pittsburgh, Pennsylvania, 15261

*** Address for Correspondence:**

Gilles Clermont

Department of Critical Care Medicine

University of Pittsburgh School of Medicine

Scaife 606B

3550 Terrace

Pittsburgh, PA 15261

Tel: (412)647-7980

Fax: (412) 647-8060

Email addresses: dauns@upmc.edu, rubin@math.pitt.edu, cler@pitt.edu

Abstract

In previous work, we developed an 8-state nonlinear dynamic model of the acute inflammatory response, including activated phagocytic cells, pro- and anti-inflammatory cytokines, and tissue damage, and calibrated it to data on cytokines from endotoxemic rats. In the interest of parsimony, the present work employed parametric sensitivity and local identifiability analysis to establish a core set of parameters predominantly responsible for variability in model solutions. Parameter optimization, facilitated by varying only those parameters belonging to this core set, was used to identify an ensemble of parameter vectors, each representing an acceptable local optimum in terms of fit to experimental data. Individual models within this ensemble, characterized by their different parameter values, showed similar cytokine but diverse tissue damage behavior. A cluster analysis of the ensemble of models showed the existence of a continuum of acceptable models, characterized by compensatory mechanisms and parameter changes. We calculated the direct correlations between the core set of model parameters and identified three mechanisms responsible for the conversion of the diverse damage time courses to similar cytokine behavior in these models. Given that tissue damage level could be an indicator of the likelihood of mortality, our findings suggest that similar cytokine dynamics could be associated with very different mortality outcomes, depending on the balance of certain inflammatory elements.

Keywords:

model identification, ensemble of models, compensatory mechanisms, dynamical systems, cytokines

1. Introduction

Biological processes are often modeled with highly nonlinear mathematical systems that contain large numbers of parameters. Nonlinearity and high-dimensional parameter spaces represent challenges in the calibration of such models to experimental data, and such data fitting is further impaired by uncertainty and variability of sparse observations (especially in settings of pre-clinical and clinical relevance)(Vodovotz et al. 2007). The ensuing inverse problem of parameter identification may be particularly ill-posed in that a large number of parameter sets can typically generate models that fit data equally well. There are two general approaches to what could constitute a satisfactory solution to the inverse problem. One option is to implement a fully stochastic estimation of a stationary distribution on parameter space, while another is the approach we adopted herein, namely the creation of an ensemble of models using constrained optimization algorithms. An ensemble of models, in contrast to a single best fitting model, can display a range of behaviors and outcomes that are consistent with given data and thus might provide insight as to mechanistic trade-offs implied by the inclusion of disparate parameter sets in the ensemble. Model complexity constitutes a major obstacle to both approaches and therefore model reduction is desirable, but not at the expense of calibration to data or violation of the underlying biology.

Researchers have typically approached the reduction problem through *ab initio* model reduction, where an attempt is made to simplify the biology represented and the corresponding complexity of the model. This approach typically reduces both the number of variables and the number of parameters included in the model. A potential pitfall, however, is that oversimplification results in the inability to relate model outcomes to underlying biological components, even at a high level. Accordingly, algorithmic and data-driven model reduction techniques are desirable. These techniques are well-developed for

statistical models, but less so for nonlinear dynamical systems. Such algorithms should aim to (1) identify minimal model structures that will provide adequate calibration and (2) within each structure, use identifiability and sensitivity analysis to reduce the number of model parameters present (Raïck et al. 2006) (Zak et al. 2003). The results of these analyses can also be used to reduce the uncertainty of parameter estimates by collecting additional experimental data optimal experimental design (Delforge et al. 1990; Peterson et al. 2001).

Our earlier works present fairly detailed models of the acute inflammatory response in diverse shock states (Chow et al. 2005; Prince et al. 2006; Lagoa et al. 2006), and the complete model building cycle of an *ab initio* reduced 8-d model of the acute inflammatory response (Roy et al. 2008), which represents the first step in the process of system identification (Ljung 1999; Walter and Pronzato 1997). The last-mentioned model includes activated phagocytic cells, pro- and anti-inflammatory cytokines, and tissue damage as a surrogate for biological impact and long-term outcome. This study established a dynamic model of the right level of complexity in that we did not obtain satisfactory fits to data with fewer variables.

The current study, taking the nonlinear dynamics of the 8-d model as its starting point, seeks to algorithmically build an ensemble of models and identify functional compensatory mechanisms present within the ensemble. Topics like parameter space reduction, parameter identifiability and model identification are common in the recent systems biology literature and several previous studies have recognized the advantages of using the mentioned techniques *in silico*. (Zak et al. 2006) We achieved the parameter space reduction in three different steps. First, we conducted a local sensitivity analysis to identify a subset of parameters that have a high impact on model outcome and capture essential characteristics of the system. (Yue et al. 2006) Second, we conducted an identifiability analysis by calculating the sensitivity dependent correlation matrix of model

parameters based on relative sensitivity matrices at given time points and identified a set of highly correlated parameters.(Jacquez and Greif 1985) We then used this information to sequentially eliminate highly correlated but less sensitive parameters from the ensuing optimization phase. This elimination was achieved by fixing these parameters to their nominal values, which have been identified in the model building cycle of our earlier work(Roy et al. 2008). This algorithmic reduction reduced the dimension of the parameter space from 46 to 18.

An ensemble of 296 models was then generated by perturbing the nominal parameter set and using the perturbations as initial estimates for a local parameter optimization. The ensemble consists of a continuum of models over a broad volume in parameter space, reflecting the existence of several complementary biological mechanisms that can compensate each other to yield model behavior that fits the cytokine data. We specifically identified several such compensatory components, the tuning of which selects from among a broad continuum of damage trajectories that are all consistent with the observed cytokine time courses. Thus, our analysis has identified biological components that may contribute to diverse mortality outcomes associated with similar inflammatory insults across different individuals.

2. Materials and Methods

2.1 *Experimental Data*

Experiments on four Sprague-Dawley rats weighing 250-300 g were performed at the University of Pittsburgh, Department of Surgery, following approval by the University of Pittsburgh's Institutional Animal Care and Use Committee, to study the acute inflammatory response to endotoxin insults at various dose levels. The rats received

lipopolysaccharide (endotoxin) at doses of 3, 6, and 12 mg/kg, intraperitoneally, and all animals survived the challenge. At time points 0, 1, 2, 4, 8, 12, and 24 hr post-dosing, blood samples were taken from each rat to measure the concentration of the inflammatory cytokines IL-6, IL-10, and TNF- α . Cytokines were measured using commercially available ELISA kits (R & D Systems, Minneapolis, MN).

These experimental data were used in the model building cycle (Roy et al. 2007) to fit the acute inflammation model and therefore to generate a first, nominal set of parameters.

2.2 Mathematical Model of Acute Inflammation

All equations and the nominal parameter set of the considered acute inflammation model are given in Roy et al. (Roy et al. 2008). The model features eight dependent variables: endotoxin concentration ($PE(t)$); the total number of activated phagocytic cells ($N(t)$, including all activated immune response cells, such as neutrophils and monocytes); a tissue (damage) marker ($D(t)$); concentrations of pro- and anti-inflammatory cytokines, such as IL-6 ($IL6(t)$), TNF- α ($TNF(t)$) and IL-10 ($IL10(t)$), respectively; a tissue driven IL-10 promoter ($Y_{IL10}(t)$); and other anti-inflammatory mediator level ($C_A(t)$), representing slow-acting anti-inflammatory and damage-fixing agents such as the cytokine Transforming Growth Factor- β 1 (TGF- β 1) and cortisol. Figure 1 shows a diagram capturing all the major interactions among the eight states.

The introduction of endotoxin in the system activates N . Once activated, N up-regulates the production/release of all inflammatory mediators (TNF- α , IL-6, IL-10, and C_A) (Freeman and Natanson 2000). The pro-inflammatory cytokines IL-6 and TNF- α exert positive feedback on the system. These cytokines further activate N , as well as up-

regulating other cytokines (Freeman and Natanson 2000; Bellingan 1999). The anti-inflammatory cytokines $IL-10$ and C_A , on the other hand, exert negative feedback on the system. They inhibit the activation of N and down-regulate other cytokines (Pretolani 1999; Pinsky 2001). Tissue damage caused by activated phagocytic cells is also taken into account in this model. The tissue marker, D , further up-regulates the activation of N (Matzinger 2002) and also contributes to an up-regulation of $IL-10$.

We estimated the values of model parameters by fitting the experimental measurements of the cytokines $IL-6$, $TNF-\alpha$, and $IL-10$ at endotoxin dose challenge levels of 3 and 12 mg/kg, simultaneously. We used the Nelder Mead simplex search method (Lagarias et al. 1998) as implemented in Matlab™ (R 2007a, © 2007, The MathWorks, Natick, MA) for optimization.

Validation of the model was performed by comparing the model predictions of the time courses of the above-mentioned cytokines at an intermediate endotoxin dose challenge level of 6 mg/kg with available data collected at specific time points at that challenge level. The values of all parameters of the inflammation model (nominal parameter set) are given in Table 1. Figure 2 and Figure 3 show the model fits (endotoxin challenge of 3 and 12 mg/kg) and model validations (endotoxin challenge of 6 mg/kg) for the observable variables $IL-6$, $IL-10$, and $TNF-\alpha$ and the non-observed/non-observable variables PE , N , D , and C_A .

2.3 Parametric Sensitivity by the Finite Difference Method

The inflammation system can be expressed as a set of N_x differential equations with N_x states (x) and M parameters (θ). We calculated the N_x by M parameter sensitivity matrix $S=(s_{i,j})$ by using the finite difference approximation method, in which the sensitivity

coefficients $s_{i,j}$ are calculated from the difference of nominal and perturbed solutions using the equation

$$s_{i,j}(t) = \frac{\partial x_i(t)}{\partial \theta_j} = \frac{x_i(\theta_j + \Delta\theta_j, t) - x_i(\theta_j, t)}{\Delta\theta_j}$$

where $i \in [1, N_x]$, $j \in [1, M]$.

To facilitate direct comparison of sensitivities to parameters having different nominal magnitudes, we calculated a normalized sensitivity coefficient (Yue et al. 2006) ($\bar{s}_{i,j}$) as

$$\bar{s}_{i,j}(t) = \frac{\partial x_i(t)}{\partial \theta_j} \cdot \frac{\theta_j}{x_i}$$

2.4 Identifiability Analysis

We used the following numerical method for checking a priori local identifiability of the parameters at a given point, based on the one given by Jacquez and Greif (Jacquez and Greif 1985):

Using the values of the parameter set $\bar{\theta}$ as nominal values, the N_x by M sensitivity matrices $S(t)$ are calculated at the time points at which measurements of the cytokines have been taken (see 2.1):

$$s_{i,j}(t_1) = \left(\frac{\partial x_i(t_1)}{\partial \theta_j} \right)_{x=x(t, \bar{\theta}), \theta = \bar{\theta}, j=1, \dots, n}$$

The matrix G is constructed by stacking the time-dependent sensitivity matrices, which yields

$$G = \begin{bmatrix} S(t_1) \\ S(t_2) \\ \vdots \\ S(t_n) \end{bmatrix}.$$

We obtained the M by M sensitivity dependent correlation matrix of the parameters, which we denote R, by first calculating the covariance matrix of G, $C = \text{cov}(G) = G^T Q G$. In general, Q is a square matrix with user supplied weighting coefficients, reflecting the possibility of weighting the matrix G with additional information. Here, we take Q to be the identity matrix. Normalization of the covariance matrix C with the geometric mean of its diagonal elements gives the sensitivity dependent correlation matrix R with elements

$$r_{i,j} = c_{i,j} / \sqrt{c_{i,i} c_{j,j}}.$$

Each parameter that is locally identifiable has a correlation strictly between -1 and +1 with each of the other parameters. Parameters that are not locally identifiable have a correlation of exactly -1 or +1 with at least one other parameter. This means that these two parameters influence the model outcome in exactly the opposite or exactly the same manner, respectively.

2.5 *Parameter space reduction*

The number of free parameters in the original M-dimensional parameter set $\bar{\theta}$ can be reduced by using the following iterative process:

1. Calculate the sensitivity dependent correlation matrix R.
2. Identify one highly correlated parameter pair (A,B).
3. If model outcome is highly sensitive to both parameters, fix neither of them and restart with step 2. Else fix the parameter in the pair to which model outcome is least sensitive at its nominal value and go back to step 1.

The process continues until no more highly correlated parameters to which model output is highly sensitive remain.

2.6 Ensemble of models

We created an ensemble of models by refitting the reduced model to the experimental data described in Section 2.1 repeatedly, starting with 250 different initial parameter vectors. These initial parameter vectors have been obtained by applying Latin Hypercube sampling to the nominal parameter set with a standard deviation of 50%. Our parameter estimation is based on a nonlinear least-squares technique in which the normalized residual is given by

$$\chi^2 = \frac{1}{\max_j (y_j)} \sum_{i=1}^N [y_i - y(t_i, \theta_1 \dots \theta_M)]^2.$$

Here, y_i and $y(t_i, \theta_1 \dots \theta_M)$ represent the data and the model prediction at the time points t_i , respectively. θ_j are the model parameters. The difference between measured data and model prediction at the given time points is normalized by $\max(y_j)$, which is the maximum value of the data over all time points. N is the number of data points and M is the total number of model parameters. Further, we used the Nelder-Mead simplex search method (Lagarias et al. 1998) as implemented in Matlab™ (v. R2007a, The Mathworks, Natick, MA) to minimize the normalized residual.

2.7 Hierarchical clustering

We use the single-linkage clustering algorithm based on a basic process of hierarchical clustering defined by Johnson(Johnson 1967) to perform a cluster analysis of our ensemble of models. In this method the distance between one cluster and another cluster is considered to be equal to the shortest distance from any member of one cluster to any member of the other cluster. Let N be a given set of items to be clustered and $D = (d[i,j])$ the $N \times N$ distance (or proximity) matrix between the N elements. The clusterings are assigned sequence numbers $0, 1, \dots, (N-1)$ and $L(k)$ is the level of the k th clustering. A cluster with sequence number m is denoted by (m) and the proximity between clusters (r)

Hierarchical clustering:

1. Begin with the disjoint clustering, which we label as having level $L(0)=0$ and sequence number $m=0$.
2. Find the least dissimilar pair of clusters in the current clustering, say (r) , (s) , according to $d[(r),(s)] = \min d[(i),(j)]$, where the minimum is over all pairs of clusters in the current clustering.
3. Increment the sequence number: $m=m+1$. Merge clusters (r) and (s) into a single cluster to form the next clustering m . Set the level of this clustering to $L(m) = d[(r),(s)]$.
4. Update the proximity matrix, D , by deleting the rows and columns corresponding to clusters (r) and (s) , respectively, and adding a row and column corresponding to the newly formed cluster. The proximity between the new cluster, denoted (r,s) , and any old cluster (k) is defined by: $d[(k), (r,s)] = \min (d[(k),(r)], d[(k),(s)])$.
5. If all objects are in one cluster, stop. Else, return to step 2

and (s) is denoted $d[(r),(s)]$. The algorithm outlined in the inset is composed and repeated until either the stopping criterion is met or $L(k)$ exceeds a tolerance. After performing a cluster analysis on the ensemble of models, we calculated the centroid of each cluster by calculating the mean of the parameter vectors in each given cluster.

2.8 Marginal distributions of parameters

Given n random variables x_1, x_2, \dots, x_n with joint probability function $f(x_1, \dots, x_n)$, the marginal distribution of x_r is obtained by integrating the joint probability density over all variables but x_r :

$$g_r(x_r) = \int_{-\infty}^{\infty} \int_{-\infty}^{\infty} \cdots \int_{-\infty}^{\infty} f(x_1, x_2, \dots, x_n) dx_1, \dots, dx_{r-1}, dx_{r+1}, \dots, dx_n.$$

The resulting function can be interpreted as a probability density of the single variable x_r .

3. Results

3.1 Sensitivity Analysis

We calculated the model sensitivity coefficients $\bar{s}_{i,j}$ as described in Section 2.3. The time points we used correspond to the time points at which measurements of the cytokines were collected (see Section 2.1). As an example, Figure 4 shows the dependence of *IL-10* on changes in each of the 46 parameters at six different time points subsequent to time 0.

We recognize that this model variable is most sensitive to the parameters 1 and 2, which are the decay rate of endotoxin and the activation rate of phagocytic cells, during the early time points (3, 4 and 5). This is a logical situation, since we assumed in the model building cycle that the first peak of *IL-10*, which happens early in time, is driven by activated phagocytic cells.

We assumed in our modeling study that the second peak in *IL-10* is driven by tissue damage working through a dynamical filter (Y_{IL10} , 2nd effect on *IL10*). Hence, it is not at all surprising, and indeed is a nice confirmation of computational accuracy, to observe that at later time points (5 and 6), *IL-10* is most sensitive to the parameters 13, 14, 15 and 46, which appear in the equations for tissue damage and Y_{IL10} .

Sensitivity dependent correlation of model parameters

The sensitivity dependent correlation matrices at an early and at a late time point (time points 3 and 7, respectively) are displayed in Figure 5A and B, while Figure 5C depicts the sensitivity dependent correlation matrix, R, summarized over all time points. Unlike other model parameters, parameters 33, 35 and 36 act independently to influence the early time course of the model outcome and parameters 13, 14 and 15 have a similarly prominent influence on the later time course.

The calculation of the sensitivity dependent correlation matrix summarized over all time points yields one pair of parameters with perfect correlation (+1 or -1 off the diagonal of the correlation matrix). Of the 1035 pairs of parameters, 163 exhibited a correlation with absolute value >0.99. The absolute correlation was <0.5 in 91 pairs of parameters and less than 0.1 for two parameters.

3.2 *Parameter space reduction*

Starting with the 163 pairs of highly correlated parameters as determined from the sensitivity dependent correlation matrix R (see 2.4 and 3.2), we reduced the parameter space from 46 to 18 dimensions, using the iterative process described in Section 2.5. The remaining 18 free model parameters appear in red in Table 1. We have observed that a similar reduction, yielding between 15 and 18 free parameters, could be obtained, by choosing a correlation cut-off between 80% and 99%, and that the rest of our results are similar for any choice in this range. The focus henceforth will be on the set of 18 parameters resulting from the 99% cut-off.

To verify that a reasonable model fit can also be obtained with the reduced model, we increased each of the 18 remaining free parameters by 50% of their nominal values and refitted the model simultaneously to the experimental data obtained from the system response to challenges of doses of 3 and 12 mg/kg of endotoxin (see 2.1). Figure 6 shows that the prediction offered by the re-optimized reduced model and original model to an endotoxin challenge of 6 mg/kg are comparable. A residual value of 0.2617 of this new fit compared with a value of 0.3355 of the original fit shows also that reducing the parameter space does not impact the quality of the model fits.

3.3 *Ensemble of models*

We created an ensemble of 102 models by refitting the reduced model to the experimental data starting with 250 different initial parameter vectors (see 2.6). The reduction from 250 initially started optimizations to 102 good fits is due to either convergence failure of the optimizer (13 cases) or convergence to a minimum with a

residual greater than 0.5 (133 cases). A residual of 0.336 in fitting our original model was the reason for choosing 0.5 as a cut-off limit.

3.4 Hierarchical clustering

We performed a cluster analysis on our ensemble of models using the single-linkage algorithm described in Section 2.7. Figure 7 shows the clustering result as a hierarchical tree. The x-axis shows the different cluster nodes (only 29 nodes are shown; the most similar models are already combined into one cluster node) and the y-axis shows the Euclidian distance between them. This direct clustering method (without normalization and sensitivity compensation) shows a division of our ensemble of 103 models (we included the original parameter set for comparison reasons) into three different clusters: the black cluster, which contains 95 models; the dark grey cluster, which contains 6 models and the light grey cluster, which contains only two of the 103 models. An alternative analysis, in which the model parameters were normalized and multiplied with their sensitivity value before the calculation of the Euclidian distance, suggests that there exists only one single cluster. A cluster analysis dependent on the maximum distance between the models yields a division of the ensemble of models into the same three clusters as the ones resulting from the cluster analysis dependent on the Euclidian distance.

Even though the direct clustering algorithm might not be an appropriate clustering method because it does not take any normalization or sensitivities into account, the calculation of the centroids of the three different clusters obtained from the direct clustering algorithm reveals an interesting fact. Figures 8A and B show the damage trajectories of the three centroids for an endotoxin challenge of 3 and 6 mg/kg, respectively. Interestingly, the three distinct clusters differ significantly in their damage behavior.

This diversity in damage trajectories, together with the fact that all models fit the *IL-6*, *IL-10* and *TNF- α* data equally well, suggests that either there are a collection of distinct mechanisms that can generate the observed data or there are one or more compensatory mechanisms leading to a continuum of models capable of producing this behavior.

3.4.1 Generation of additional models

To ascertain whether a continuum of models based on compensatory mechanisms exists or whether distinct mechanisms are responsible for the coexistence of the diverse damage and the similar cytokine behavior, we generated 193 additional models using the method described in Section 2.6, starting from the centroids of the dark (97 models) and light grey clusters (96 models).

3.4.2 Clustering result on 296 models

Figure 9A shows the result of the direct clustering method (clustering is only based on the Euclidian distance). Figure 9B shows the cluster result after model parameters have been normalized and multiplied with their corresponding sensitivity values before the Euclidian distance was calculated. In both cases 295 models form a continuum over a broad distance in parameter space, as would be expected from the continuous tuning of one or more compensatory mechanisms. A single other model forms its own cluster. Figures 8C and D show the continuum of predicted damage trajectories in the case of an endotoxin challenge of 3 and 6 mg/kg.

This result suggests that the different cluster results obtained by applying both clustering algorithms to the ensemble of 103 models emerged from consideration of an insufficient diversity of parameter values.

3.5 *Compensatory mechanisms*

To investigate which of the remaining 18 parameters of the reduced model are responsible for compensating for the diverse damage behavior, we calculated the covariance matrix of these parameters directly, across the ensemble of 296 models. As with the sensitivity dependent correlation matrix computed earlier, we normalized by the geometric mean of the diagonal elements. We emphasize that, in contrast to the correlation matrix of all original 46 parameters calculated in Section 3.2, this calculation was based on the values of parameters, not the sensitivities of model outcomes to their values. The result is shown in Figure 10. This Figure has been produced by plotting the surface formed by linear interpolation between values of the correlation coefficients followed by projection of this surface back to the parameter – parameter plane. For each colored square, each vertex describes the correlation between a different parameter pair. The color of the square is determined by the highest correlation value of the four different parameter pairs represented at its vertices. For each white square, at least one of the vertices corresponds to a highly correlated parameter pair, and in each case, the identity of this vertex was determined by direct inspection of correlation values.

The parameter pairs $k_D - x_{IL102}$, $x_D - x_{IL10}$ and $k_{CA} - x_{TNFCA}$ exhibit a correlation greater than 0.8. Figure 11 shows the scatter plots of these three parameter pairs (A, B and C) and the scatter plot of one parameter pair exhibiting an absolute correlation smaller than 0.02 (D). The high positive correlation between the parameter pairs k_D and x_{IL102} and x_D and x_{IL10} tells us that differences in the damage trajectory produced by

changes in damage generation k_D or by changes in the damage saturation constant x_D are compensated by the dynamical filter Y_{IL10} (Eq. 21, Roy et al. 2008), since damage drives the second surge in $IL-10$ production as captured by the variable Y_{IL10} , or by the saturation constant of the basic production of $IL-10$, respectively. A high positive correlation between the parameters k_{CA} and $x_{TNF\alpha}$ means that differences in the anti-inflammatory mediator (C_A) trajectory produced by changes in k_{CA} are compensated by the downregulation of $TNF-\alpha$ by C_A .

The marginal distributions of all 18 parameters have been calculated and those for parameters in the three highly correlated parameter pairs are shown in Figure 11. The finding that the marginal distributions of the correlated parameters are not uniform may reflect an indirect effect of other model parameters on these compensatory mechanisms, or vice versa.

4. Discussion

In this work we reduced the 46 dimensional parameter space of an 8 state mathematical model of the acute inflammatory response to 18 dimensions using parameter sensitivity and local identifiability analysis. We verified that the solutions of the reduced model exhibit qualitatively similar dynamics to the solutions of the full model and provide a similarly good fit to experimental data. We created an initial ensemble of 103 parameter vectors providing a good fit to experimental data by calibrating to experimental data using only the core parameters. The hierarchical cluster analysis of the ensemble of 103 models suggested that the ensemble could be classified into three clusters. However, an alternative clustering that takes a normalization of model parameters and their sensitivities into account eliminated this clustering. Nonetheless, an important

observation is that the centroids of the three original clusters all lead to good fits to experimental data but with diverse damage time courses. This diversity in damage outcomes, together with the fact that all models fit the *IL-6*, *IL-10* and *TNF- α* data equally well, suggested either that the model includes multiple distinct mechanisms that produce behavior consistent with the data or that the model features compensatory parameter pairs that allow a particular set of mechanisms to work across a diverse range of parameter values, as long as certain parameters covary. To distinguish between these possibilities, we used parameter optimization from additional starting points to increase the number of models in the ensemble to 296. Cluster analysis showed that this expanded ensemble included a continuum of models yielding similar cytokine time courses, revealing the presence of compensatory mechanisms within our mathematical representation of the acute inflammatory response. Indeed, we identified the three particular mechanisms that provide the strongest compensation by investigating the correlations between the 18 parameters in the reduced parameter set

As stated in the introduction, algorithms set up for model complexity reduction should aim to (1) identify minimal model structures that will provide adequate calibration and (2) within each structure, reduce the number of parameters using identifiability and sensitivity analysis. Since our earlier work suggested that the model of the inflammatory response would lose validity under further state reduction, we focused here on simplifying the inverse or data fitting problem by reducing the parameter space. The approach we used for the reduction of the parameter space fits well into the current literature (Zak et al. 2003; Rodriguez-Fernandez et al. 2006; Joseph et al. 2002; Chang et al. 2005). For example, in previous work, identifiability analysis has been applied in studies of ligand binding (Delforge et al. 1990) and water treatment (Peterson et al. 2001) to investigate how additional perturbations or measurements improve the accuracy of parameter estimates.

In theory, we could have attempted to further reduce the set of 18 parameters varied in our data fitting procedure. In particular, the reduced parameter set that we obtained by applying the parameter space reduction technique still contains several non-correlated, non-sensitive parameters. We did not fix those parameters, however, because it might well be the fact that a non-sensitive parameter becomes more important for model outcome as other parameters are varied or if the value of the parameter itself is varied dramatically. That is, the sensitivity analysis we applied gives only results that are local in parameter space. Hence, the use of correlations in sensitivities is crucial to our approach, and the question whether non-correlated, non-sensitive parameters should be fixed to their nominal values to reduce the parameter space even further has to be answered carefully using other diagnostics.

Clearly, in the absence of damage data, it is important not to fix parameters in the three correlated pairs responsible for the compensatory model behavior, since such a restriction would automatically constrain the second parameter in each pair, leading to a single model behavior instead of a continuum. If information about damage becomes available, then these parameters would represent natural handles to use in fitting that data. Interestingly, the fact that the marginal distributions of the correlated parameters responsible for the compensatory model behavior are not uniform suggests that additional parameters interact with the six parameters specifically identified as providing compensation. The suggestion of such balancing mechanisms has considerable biological face validity, although those identified herein remain hypothetical.

Although we could possibly have overlooked biologically relevant regions of parameter space, we are confident we explored the parameter space of the mathematical model exhaustively since we identified a continuum of models by refitting the nonlinear mathematical model starting from initial parameter guesses obtained by a 50% disturbance of the nominal parameter set. To further verify the thoroughness of our

search, we are currently applying a stochastic method based on an adaptive Markov Chain Monte Carlo algorithm as an alternative approach to the creation of an ensemble of models for this system. This algorithm will search a much larger volume of parameter space.

It must also be emphasized that all models in our ensemble have been calibrated to mean experimental data and not to individual animals. Before we calculated the mean of the experimental observations, we verified that the cytokine response is consistent across all animals (i.e. a second surge in IL-10 was observed in every animal). Therefore, predictions from an ensemble such as the one we created are most relevant to cohort behavior and not individual behavior. Yet, proper subsets of the ensemble could be selected as to include known heuristics of subpopulations of animals. For example, using the area under the damage curve as a measurement for model outcome (death or health), a subset of the ensemble of models could be selected to simulate the behavior of a rat population exhibiting a given mortality. Of course, the subset selection procedure could be adjusted as additional information about the distribution of initial conditions across the population becomes available. In particular, the quantitative fits obtained would change if we had additional data from animals that did not survive the endotoxin challenge. Future work will explore the use of individual time course data in the generation of an ensemble of models.

The derivation of computationally tractable models of biological systems, which are sufficiently reduced to provide insight into mechanisms underlying system behavior, typically requires identification of a key set of minimal components to be modeled, irrespective of the particular scale addressed by the model. For many systems, however, *ab initio* reduction still yields a potentially severely underconstrained system. The methods presented herein (1) suggest a tractable, effective method to reduce parameter space while maintaining a good fit to experimental data, and (2) identify diverse, possibly

compensatory dynamic mechanisms contributing to these fits. Therefore, we expect such an approach to be of broad applicability to future work on the modeling of biological systems.

Acknowledgements

This work was supported by the National Institutes of Health grants R01-HL-76157-02, RO1-HL-076157-02, R01-DC-008290, and P50-GM-53789-09.

References

1. Bellingan, G. 1999. Inflammatory cell activation in sepsis. *Br Med Bull* 55, 12-29.
2. Chang, S. T., Linderman, J. J., and Kirschner, D. E. 2005. Multiple mechanisms allow *Mycobacterium tuberculosis* to continuously inhibit MHC class II-mediated antigen presentation by macrophages. *Proc Natl Acad Sci U.S.A* 102(12), 4530-4535.
3. Chow, C. C., Clermont, G., Kumar, R., Lagoa, C., Tawadrous, Z., Gallo, D., Betten, B., J. Bartels, Constantine, G., Fink, M. P., Billiar, T. R., and Vodovotz, Y..

2005. The acute inflammatory response in diverse shock states. *Shock* 24(1), 74-84.
4. Delforge, J., Syrota, A., and Mazoyer, B. M. 1990. Identifiability analysis and parameter identification of an in vivo ligand-receptor model from PET data. *IEEE Trans Biomed Eng* 37, 653-661.
 5. Freeman, B. D. and Natanson, C. 2000. Anti-inflammatory therapies in sepsis and septic shock. *Expert Opin Investig Drugs* 9, 1651-1663.
 6. Jacquez, J. A. and Greif, P.. 1985. Numerical parameter identifiability and estimability: Integrating identifiability, estimability, and optimal sampling design. *Math Biosci* 77, 201-227.
 7. Johnson, S. C. 1967. Hierarchical clustering schemes. *Psychometrika* 2, 241-254.
 8. Joseph, I. M. P., Zavros, Y., Merchant, J. L., and Kirschner, D. 2002. A model for integrative study of human gastric acid secretion. *J Appl Physiol* 94, 1602-1618.
 9. Lagarias, J. C., Reeds, J. A., Wright, M. H., and Wright, E. 1998. Convergence properties of the Nelder-Mead simplex method in low dimensions. *SIAM Journal of Optimization* 9(1), 112-147.
 10. Lagoa, C. E., Bartels, J., Baratt, A., Tseng, G., Clermont, G., Fink, M. P., Billiar, T. R., and Vodovotz, Y. 2006. The role of initial trauma in the host's response to injury and hemorrhage: Insights from a comparison of mathematical simulations and hepatic transcriptomic analysis. *Shock* 26, 592-600.

11. Ljung, L. 1999. System identification - Theory for the user. 2nd ed, PTR Prentice Hall, Upper Saddle River, N.J.
12. Matzinger, P. 2002. The danger model: a renewed sense of self. *Science* 296(5566), 301-305.
13. Peterson, B., Gernaey, G., and Vanrolleghem, P. A. 2001. Practical identifiability of model parameters by combined respirometric-titrimetric measurements. *Water Sci Technol* 43, 347-355.
14. Pinsky, M. R. 2001. Sepsis: a pro- and anti-inflammatory disequilibrium syndrome. *Contrib Nephrol* 132, 354-366.
15. Pretolani, M. 1999. Interleukin-10: an anti-inflammatory cytokine with therapeutic potential. *Clin Exp Allergy* 29, 1164-1171.
16. Prince, J. M., Levy, R. M., Bartels, J., Baratt, A., Kane, J. M., Lagoa, C., Rubin, J., Day, J., Wei, J., Fink, M. P., Goyert, S. M., Clermont, G., Billiar, T. R., and Vodovotz, Y. 2006. In Silico and In Vivo Approach to Elucidate the Inflammatory Complexity of CD14-deficient Mice. *Mol Med*.
17. Raick, C., Soetaert, K., and Gregoire, M. 2006. Model complexity and performance: How far can we simplify? *Progress in Oceanography* 70(1), 27-57., doi:10.1016/j.pocean.2006.03.001.
18. Rodriguez-Fernandez, M., Mendes, P., and Banga, J. R. 2006. A hybrid approach for efficient and robust parameter estimation in biochemical pathways. *Biosystems* 83(248), 265., doi:10.1016/j.biosystems.2005.06.016.

19. Roy, A., Clermont, G., Daun, S., and Parker, R. S. 2007. A Mathematical Model of the Acute Inflammatory Response to Endotoxin Challenge. Abstract, AIChE Annual Meeting, Salt Lake City, UT, paper 538g.
20. Roy, A., Clermont, G., Daun, S., Rubin, J., Vodovotz, Y., and Parker, R. S. 2008. A mathematical model of acute inflammatory response to endotoxin challenge. IEEE Transactions on Biomedical Engineering submitted.
21. Vodovotz, Y., Clermont, G., Hunt, C. A., Lefering, R., Bartels, J., Seydel, R., Hotchkiss, J., Ta'asan, S., Neugebauer, E., and An, G. 2007. Evidence-based modeling of critical illness: an initial consensus from the Society for Complexity in Acute Illness. *J.Crit Care* 22(1), 77-84.
22. Walter, E. and Pronzato, L. 1997. Identification of Parametric Models from Experimental Data. Springer-Verlag, London.
23. Yue, H., Brown, M., Knowles, J., Wang, H., Broomhead, D. S., and Kell, D. B. 2006. Insights into the behaviour of systems biology models from dynamic sensitivity and identifiability analysis: a case study of an NF-kB signalling pathway. *Mol Biosyst* 2, 640-649.
24. Zak, D. E., Gonye, G. E., Schwaber, J. S., and Doyle, F. J. III. 2003. Importance of Input Perturbations and Stochastic Gene Expression in the Reverse Engineering of Genetic Regulatory Networks: Insights from an Identifiability Analysis of an In Silico Network. *Genome Res* 13, 2396-2405.

Figures

No	Parameter	Value	Unit	No	Parameter	Value	Unit
1	d_{PE}	3	hr ⁻¹	24	$X_{IL6IL10}$	1.1818	pg/ml
2	k_N	5.5786e7	hr ⁻¹	25	k_{IL6IL6}	122.92	
3	X_N	14.177	N-unit	26	X_{IL6IL6}	1.987e5	pg/ml
4	d_N	0.1599	hr ⁻¹	27	X_{IL6CA}	4.2352	pg/ml
5	k_{NPE}	41.267	N-unit*kg/mg	28	k_{TNF}	3.9e-8	pg/(ml*N-unit ^{1.5})
6	k_{ND}	0.013259	N-unit/D-unit	29	d_{TNF}	2.035	hr ⁻¹
7	X_{NTNF}	1693.9509	pg/ml	30	$X_{TNFIL10}$	2.2198e7	pg/ml
8	X_{NIL6}	58080.742	pg/ml	31	X_{TNFCA}	0.19342	pg/ml
9	X_{NCA}	0.07212	pg/ml	32	k_{TNFTNF}	1.0e-10	
10	X_{NIL10}	147.68	pg/ml	33	X_{TNFTNF}	9.2969e6	pg/ml
11	k_{NTNF}	12.94907		34	X_{TNFIL6}	55610	pg/ml
12	k_{NIL6}	2.71246		35	$k_{IL10TNF}$	2.995e-5	
13	k_D	2.5247	D-unit/hr	36	$X_{IL10TNF}$	1.1964e6	pg/ml
14	d_D	0.37871	hr ⁻¹	37	$k_{IL10IL6}$	4.1829	
15	X_D	1.8996e7	N-unit	38	$X_{IL10IL6}$	26851	pg/ml
16	k_{CA}	1.5463e-9	pg/(ml*hr*N-unit)	39	k_{IL10}	1.3374e5	pg/(ml*hr)
17	d_{CA}	3.1777e-2	hr ⁻¹	40	d_{IL10}	98.932	hr ⁻¹
18	S_{CA}	0.004	pg/(ml*hr)	41	X_{IL10}	8.0506e7	N-unit
19	k_{IL6TNF}	3.7209		42	S_{IL10}	1187.2	pg/(ml*hr)
20	X_{IL6TNF}	1211.3	pg/ml	43	X_{IL10d}	791.27	pg/ml
21	k_{IL6}	8.8652e7	pg/(ml*hr)	44	k_{IL102}	1.3964e7	Y_{IL10} -unit/hr
22	d_{IL6}	0.43605	hr ⁻¹	45	d_{IL102}	0.024943	hr ⁻¹
23	X_{IL6}	1.7856e8	N-unit	46	X_{IL102}	37.454	D-unit

Table 1: Nominal parameter set of the inflammation model.

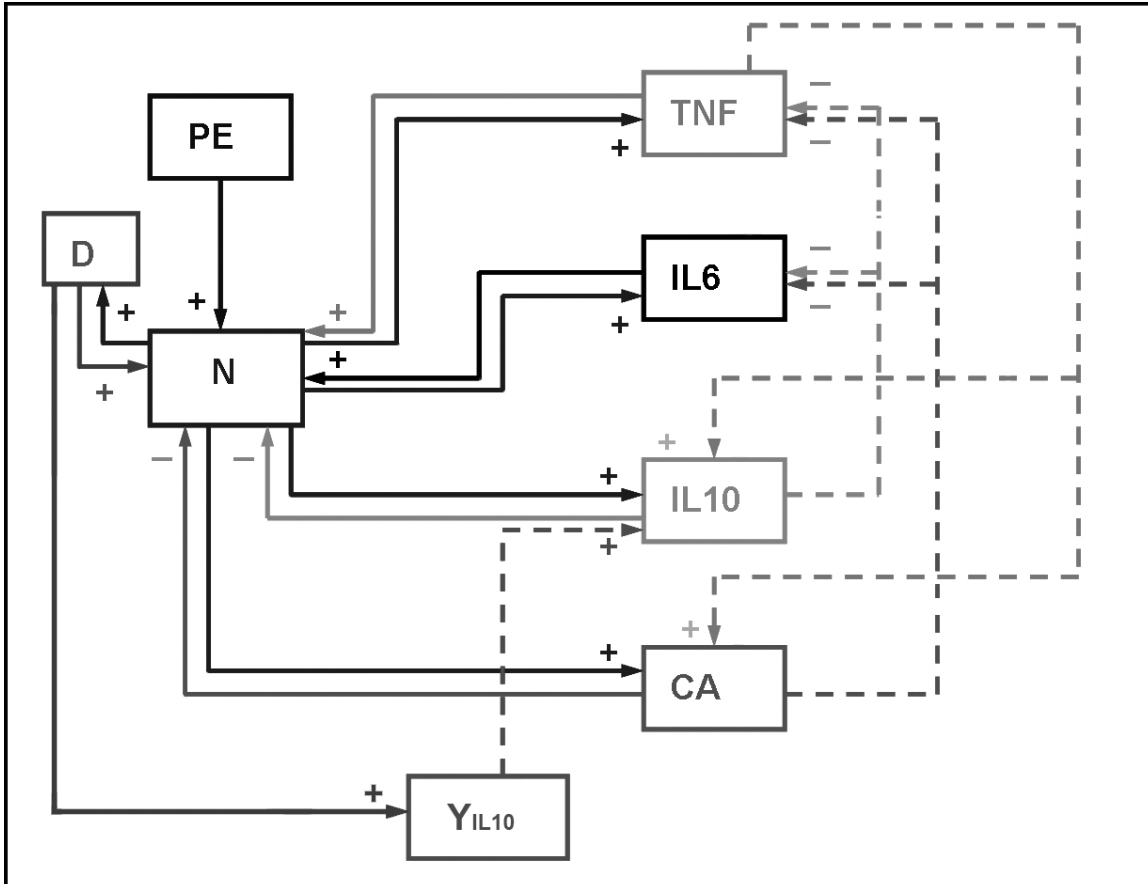


Figure 1: Schematic diagram of the inflammatory response system challenged by endotoxin.

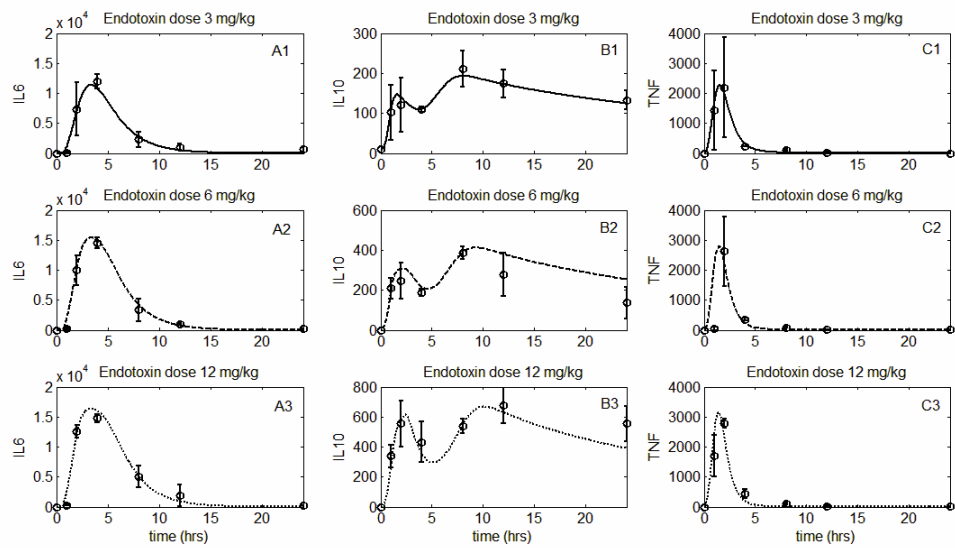


Figure 2: The observable states of the inflammatory response to endotoxin challenge. The curves show simulated time courses of several components of the inflammatory response to endotoxin challenge, namely *IL-6*, *IL-10* and *TNF-α*. The discrete points indicate levels of these elements measured experimentally; error bars representing one standard deviation about the mean are also shown. Endotoxin challenge levels were 3 (top), 6 (middle), and 12 (bottom) mg/kg.

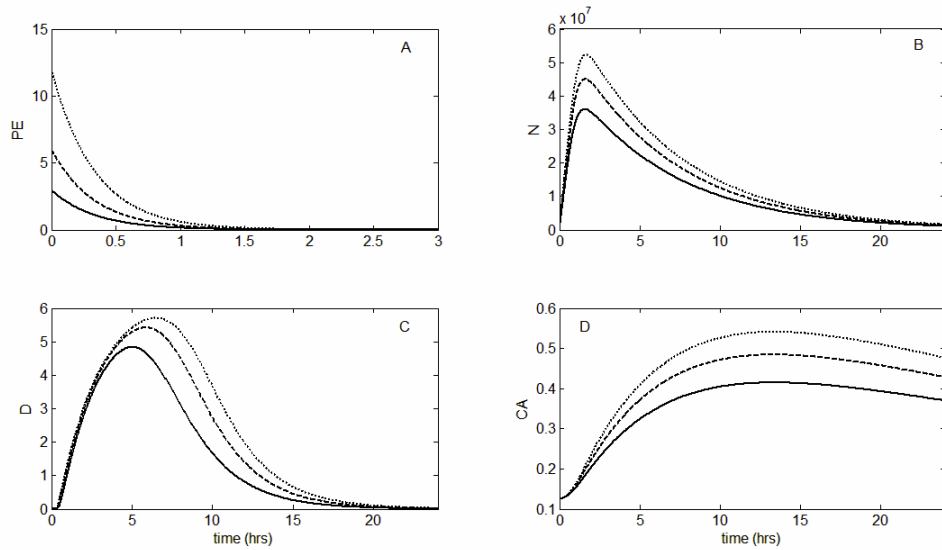


Figure 3: Non-observable states of the model inflammatory response to endotoxin challenge. Simulated time courses of the non-observable variables D and C_A and the non-observed variables PE and N for different endotoxin challenges (solid: 3 mg/kg, dashed: 6 mg/kg and dotted: 12 mg/kg) are shown. Note that the time scale of PE goes from 0 to 3 hrs, whereas the time scales of N , D , and C_A go from 0 to 24 hrs.

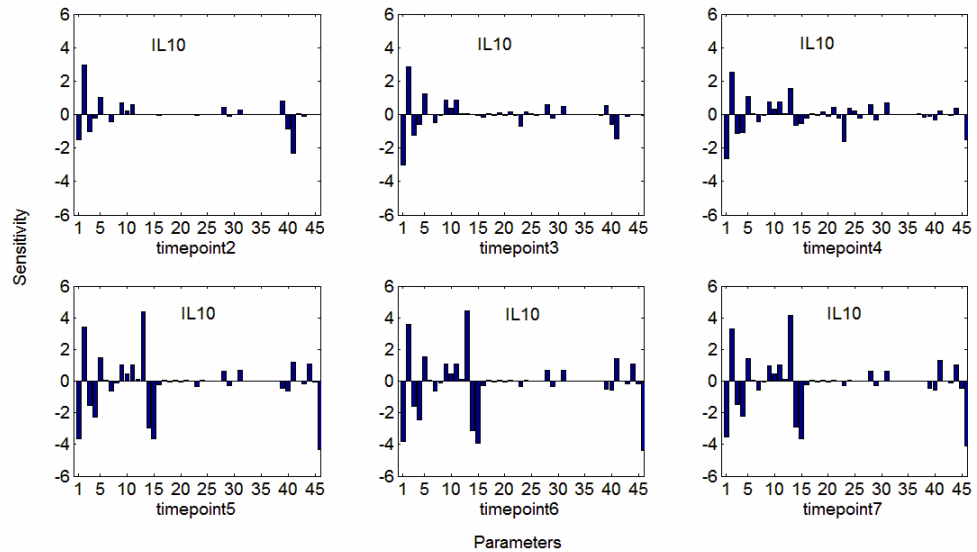


Figure 4: Sensitivity analysis. Sensitivities of *IL-10* to changes in each of the 46 model parameters were determined at several time points at which measurements of the cytokines were collected. Timepoints 2 through 7 correspond to measurements taken at 1, 2, 4, 8, 12, and 24 h after endotoxin challenge (see Section 2.1). The higher the absolute value of the sensitivity, the more sensitive *IL-10* is to the corresponding model parameter.

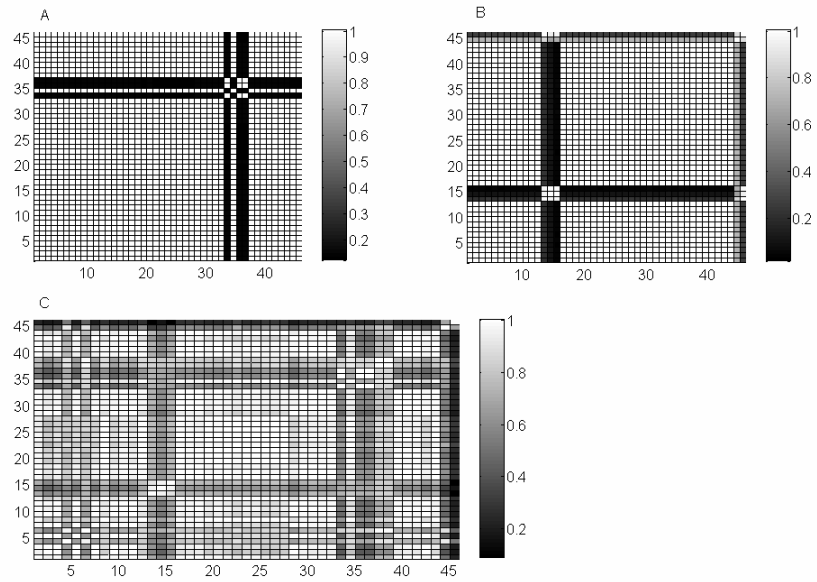


Figure 5: Sensitivity-dependent correlation matrix containing the correlation coefficients of the 46 model parameters at A) an early time point and B) a late time point. C) Sensitivity dependent correlation matrix summarized over all seven time points.

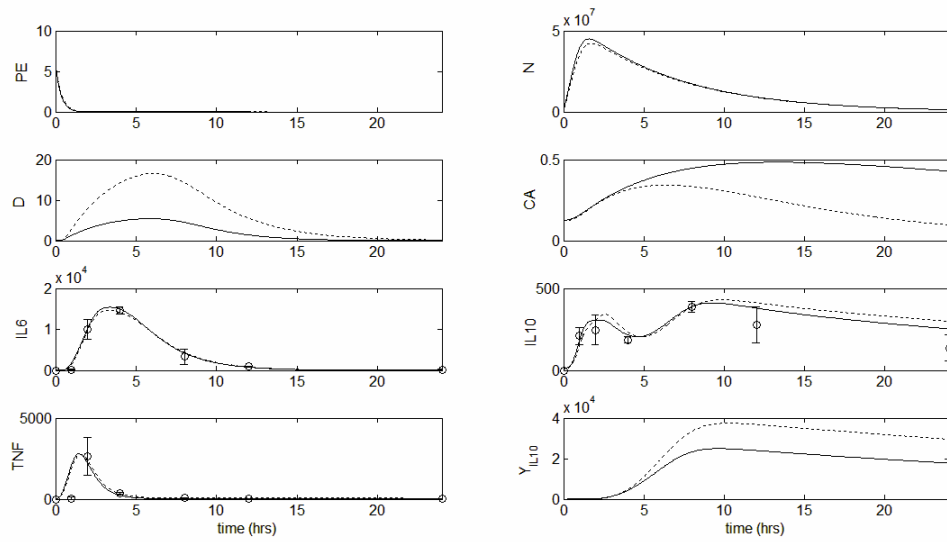


Figure 6: Simulated time courses of the 8 state variables of the inflammation model for an endotoxin challenge of 6 mg/kg. The solid line shows the inflammatory response simulated with the nominal parameter set and the dashed line shows the inflammatory response simulated with the parameter set obtained after refitting the reduced model, with only 18 parameters, to the experimental cytokine data.

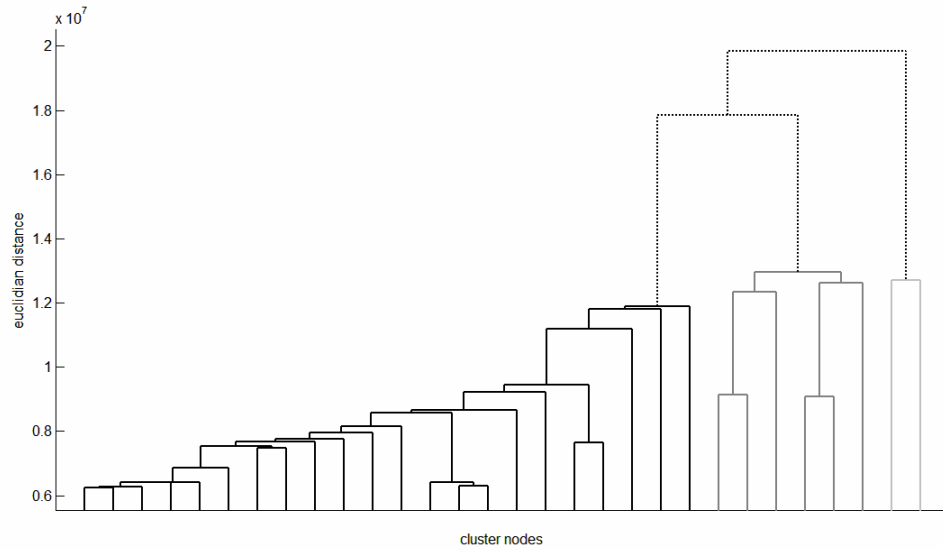


Figure 7: Cluster tree of the ensemble of 103 models. Only 29 cluster nodes are shown, because the most similar models are already comprised into single nodes. This tree suggests a natural division of the ensemble of models into three distinct clusters.

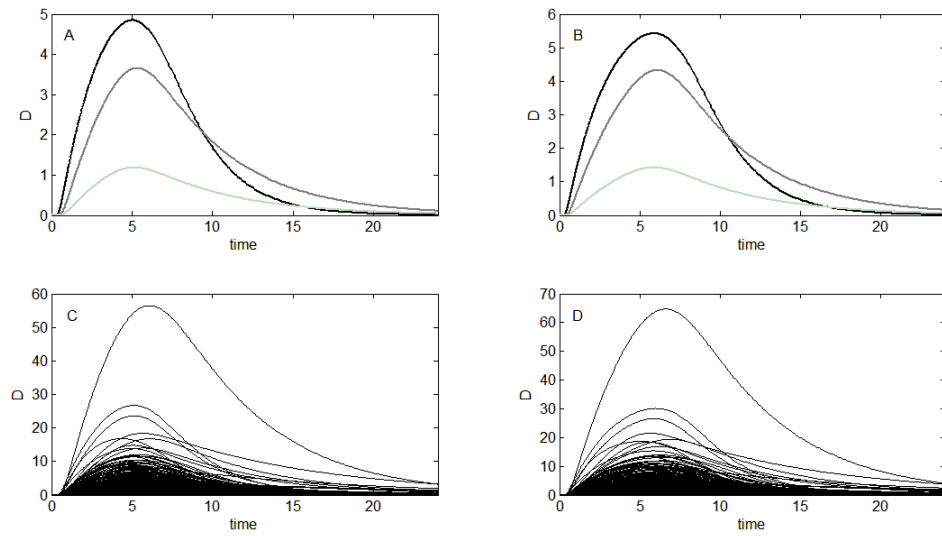


Figure 8: A) and B) Damage trajectories of the centroids of the three different clusters for an endotoxin challenge of 3 (left) and 6 (right) mg/kg, respectively. The used black and grey colors correspond to the ones of the cluster tree in Figure 7. C) and D) Damage trajectories of the continuum of 296 models for an endotoxin challenge of 3 (left) and 6 (right) mg/kg, respectively.

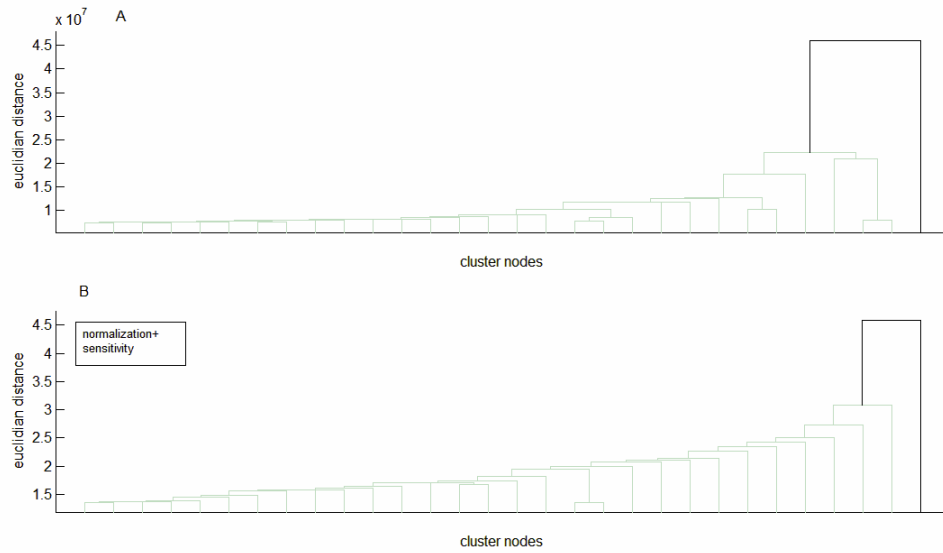


Figure 9: Cluster results of the ensemble of 296 models represented by cluster trees. A) Clustering is only based on Euclidian distance between the models, B) Model parameters have been normalized and multiplied with their corresponding sensitivity values before the Euclidian distance has been calculated. In both cases 295 models form a continuum of models based on compensatory mechanisms.

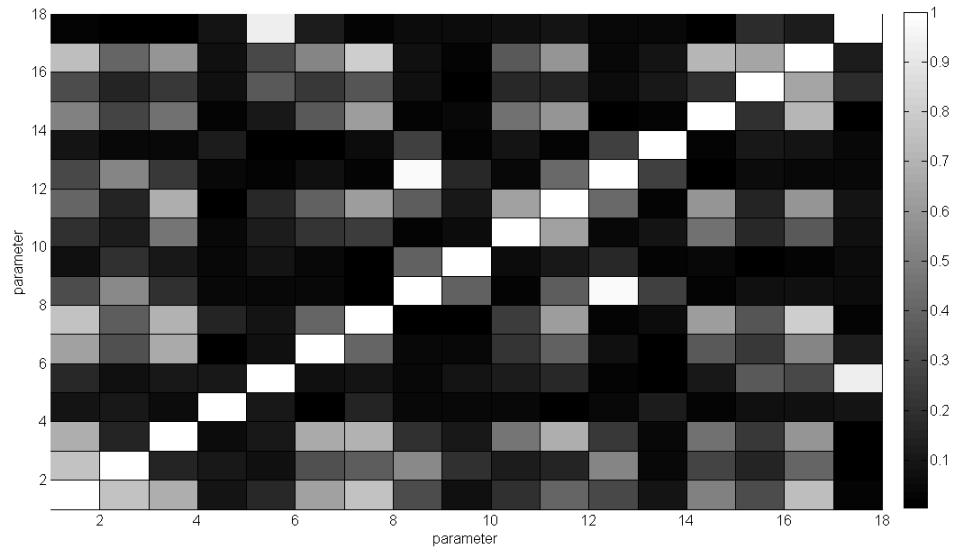


Figure 10: Direct correlation matrix of the 18 parameters in the reduced parameter set.

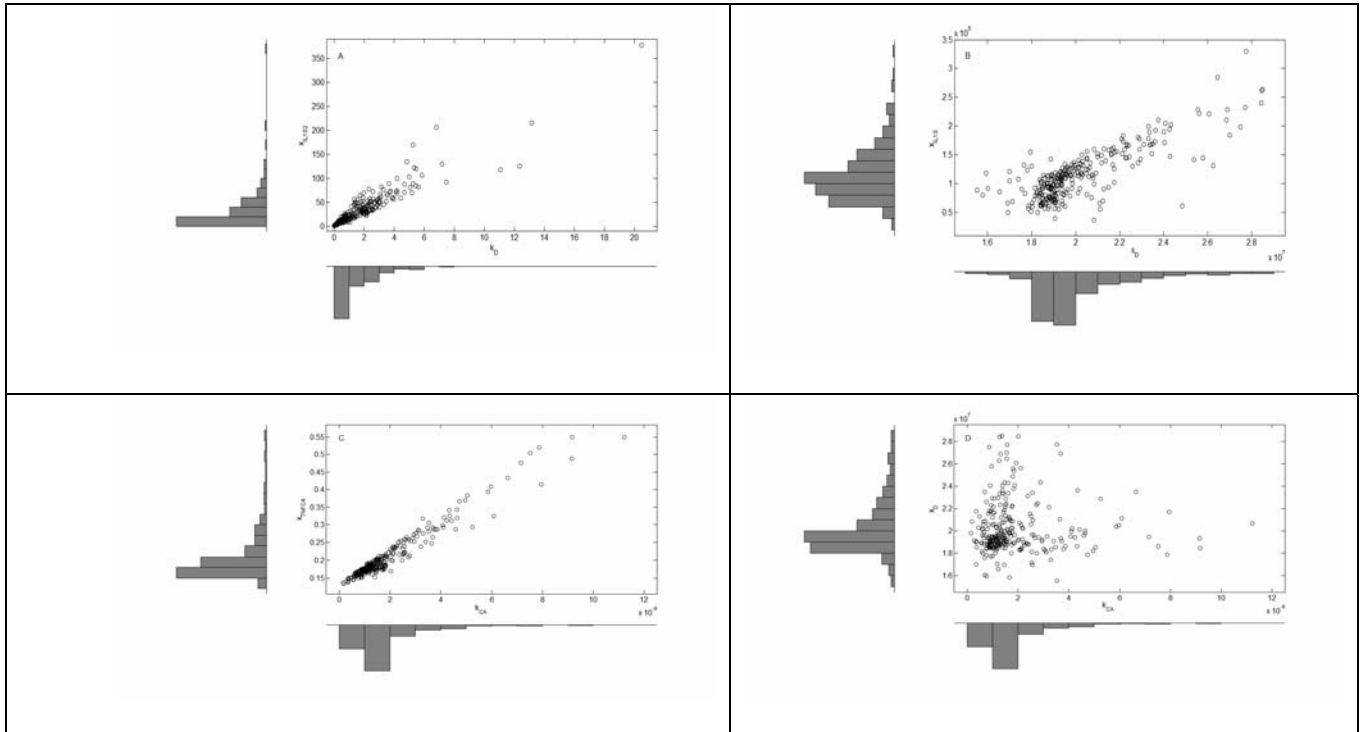


Figure 11: Non-uniform distributions of compensatory parameter pairs. The scatter plots of the three correlated compensatory parameter pairs (A, B and C) and one uncorrelated parameter pair (D) are shown, together with the marginal distribution of each parameter.

